IEEE Access
Multidisciplinary ⋮ Rapid Review ⋮ Open Access Journal

Received 24 March 2024, accepted 6 May 2024, date of publication 14 May 2024, date of current version 6 June 2024.

Digital Object Identifier 10.1109/ACCESS.2024.3400910

RESEARCH ARTICLE

Investigation on Thermal Characteristics and Performance of Cylindrical Lithium-Ion Battery Pack Using P2D Model With Varied Electrode Chemistries

P. MANGAIYARKARASI AND R. JAYAGANTHAN
Department of Engineering Design, Indian Institute of Technology (IIT) Madras, Tamil Nadu, Chennai 600036, India
Corresponding authors: P. Mangaiyarkarasi (mangaipadma@gmail.com) and R. Jayaganthan (edjay@iitm.ac.in)

This work was supported by Indus Towers Ltd., Gurugram, Haryana, India, under Grant CR22231212EDINDT008921.

ABSTRACT Efficient heat dissipation in lithium-ion battery packs is crucial for safety, necessitating a thorough assessment of thermal performance during the design phase. This study utilizes Newman's Pseudo two-dimensional (P2D) model and three-dimensional computational fluid dynamics to depict heat generation and dissipation. The main objectives include evaluating heat dynamics, establishing optimal temperature limits, and assessing State of Charge (SOC) and State of Health (SOH) estimations. The battery pack, configured in 6s2p, features plastic-wrapped cylindrical modules with air-filled domains, connected in parallel pairs with aluminum wires. Active materials comprise positive electrodes like Lithium Cobalt Oxide (LCO), Lithium Nickel Manganese Cobalt Oxide (NMC), Lithium Iron Phosphate (LFP), and Lithium Manganese Oxide (LMO), with graphite as the negative electrode and a separator (Lithium Hexa Fluoro Phosphate). Results indicate that air-cooled NMC electrode chemistry achieves a peak heat dissipation of 102.48W, maintaining an optimal temperature range of 21.3deg C to 32.8deg C. After 1000 cycles, the optimal temperature limit of 32.8deg C with an 80% capacity loss minimizes negative impacts during charge/discharge cycles. SOC and SOH remain at 100% and 80%, utilizing an 8Ah battery with a nominal voltage of 4.2V, and a 3.9-year life expectancy, addressing charge/discharge cycle issues.

INDEX TERMS Battery pack, battery life span, capacity fade, P2D model, SOC.

NOMENCLATURE

A	Area [m^2].
c_p	Specific heat [J /kg.K].
c_e	Electrolyte lithium concentration.
c_s	Solid lithium concentration.
$c_{s,p,max}$	Maximum Li+ concentration of (+) electrode in solid phase.
$c_{s,n,max}$	Maximum Li+ concentration of (-) electrode in solid phase.
D_s	Diffusion coefficient in electrolyte phase.
D_e^{eff}	Effective diffusion coefficient.
E_d	Activation energy for controlling temperature sensitivity of D_s.
E_r	Activation energy for controlling temperature sensitivity of km.
$f_{\pm}$	Coefficient of electrolyte activity.
F	Faraday's constant [Columb /mol].
i_0	Exchange current density [A/m^2].
I	Current [A].
j^{Li}	Current transmission at the electrolyte interface [A/m^2].
K	Ionic conductivity (electrolyte phase) [S /m].
k_p	Positive electrode constant reference rate.
k_n	Negative electrode constant reference rate.
$k_{m,ref}$	Reference reaction coefficient.
k_{eff}	Effective diffusional conductivity [S /m].
D	Effective ionic conductivity [S /m].
N	Number of cycles.

The associate editor coordinating the review of this manuscript and approving it for publication was Wei Xu.

P	Pre-exponential factor.
$\dot{q}$	Rate of heat generation [W].
r_0	Radial coordinate.
R	Universal gas constant [kJ /kg.mol.K].
R_s	Radius of solid active material [μm].
$R_{s,p}$	Radius of (+) electrode in solid phase [μm].
$R_{s,n}$	Radius of (−) electrode in solid phase [μm].
a_s	interfacial surface area which depends on the solid phase volume fraction.
L_{an}, L_{sep}, L_{ca}	anode, separator and cathode thicknesses.
T	Temperature [deg C].
t_+^0	Lithium transfer number.
t	Time [s].
U	Open circuit potential [V].
V	Cell voltage [V].
$SOC_{initial}$	initial SOC at the beginning of the charge or discharge cycle (%).
I(t)	current flowing in or out of the battery at time t.
A	Amps.
Ah	Ampere Hour.
Min	Minimum.
Max	Maximum.
$\int_0^t I\,(t)\,dt$	integral of the current over time (Ah).
$Q_{battery}$	Battery's rated capacity (Ah).
$Q_{battery}$(Final)	Remaining battery capacity at the end of charge or discharge cycle (Ah).
W	Watt.
Wh	Watt Hour.
deg C	Degree celcius.

A. SYMBOLS

α	Thermal diffusivity [m^2 /s].
α_a	Transfer coefficient for anode.
α_c	Transfer coefficient for cathode.
α_t	Time exponent factor.
β	Time exponent factor.
∇	Bruggeman porosity exponent.
ε_e	Gradient.
ε_s	Electrolyte volume fraction in electrolyte phase.
ε_f	Filler fraction.
η	Over potential.
ρ	Density [kg /m^3].
σ_+	Electrical conductivity for (+) electrode [S/m].
σ_-	Electrical conductivity for (-) electrode [S/m].
σ^{eff}	Effective electrical conductivity [S /m].
φ_s	Potential at solid phase [V].
φ_e	Potential at electrolyte phase [V].

B. SUBSCRIPTS

∞	Ambient.
0	Initial.
a	Anode.
c	Cathode.
e	Electrolyte.
f	Filler.
n	Negative electrode.
oc	Open Circuit.
p	Positive electrode.
ref	Reference.
s	Separator.
tot	Total.

C. SUPERSCRIPTS

Li	Lithium.
Eff	Effective.
ECH	Electrochemical heat.

D. ABBREVIATIONS

ANN	Artificial Neural Network.
BTM	Battery Thermal Management.
BTMS	Battery Thermal Management Systems.
C-rate	Charge rate or Capacity rate.
CC	Constant current.
CV	Constant voltage.
DOD	Depth of Discharge.
ECM	Electrochemical Modeling.
LCO	Lithium Cobalt Oxide.
LFP	Lithium Iron Phosphate.
Li-ion	Lithium-ion.
LMO	Lithium Manganese Oxide.
NMC	Nickel Manganese Cobalt Oxide.
OCV	Open Circuit Voltage.
p	Parallel.
P2D	Pseudo two-dimensional.
PCM	Phase Change Material.
s	Series.
SOC	State of Charge.
SOD	State of Discharge.
SOH	State of Health.

I. INTRODUCTION

Storing energy from renewable sources presents challenges due to issues related to varying energy demand and irregularities. The utilization of batteries emerges as a solution to meet the global energy storage needs, with a growing segment of the battery market due to environmental concerns. Li-ion batteries have witnessed substantial growth in the energy storage sector due to its high energy density, extended lifespan, and efficient charge retention. However, a significant drawback is the generation of substantial heat during charge and discharge cycles [1]. Maintaining appropriate temperatures is pivotal for safety and performance [2], as high temperatures can lead to battery capacity loss and even thermal runaway. Effective thermal management of battery pack is thus essential to ensure its safe operating temperatures [3]. Improving BTM has become the focus of various research efforts worldwide.

Vayrynen and Salminen [4] proposed an optimal temperature range of -20deg C to 60deg C for Li-ion cells. Jiang et al. [5] emphasized a safety limit of 50deg C and highlighted the importance of minimizing temperature variations within a battery module should not be more than 5deg C. Proper thermal modeling plays a vital role in maintaining suitable working temperatures and temperature uniformity within Li-ion batteries, necessitating an understanding of heat generation within these batteries [6].

Accurate measurement or estimation of heat generation within batteries is crucial for precise temperature control. Numerical models, including electrochemical [7], [8], electro-thermal [9], [10] and lumped models [11], [12], have also been developed to estimate heat generation. Chen et al. [13] compared lumped and electrochemical models, favoring the uniform temperature predictions of the lumped model, although it's unsuitable for predicting temperature variations.

Xie et al. [14] critiqued electro-thermal models for ignoring physicochemical principles and assuming uniform temperature distribution. Doyle et al. [15] introduced the P2D model, a physics-based ECM capable of accurately predicting Li-ion movement. Numerous studies have employed the P2D model to simulate heat generation in Li-ion batteries. Panchal et al. [8] utilized the P2D model to compute battery temperature and voltage during discharging, achieving agreement with experimental data. Saw et al. [16] demonstrated accuracy of the P2D model in both charging and discharging scenarios.

Effective battery cooling system design has been crucial, especially under challenging conditions like extreme heat or rapid charge/discharge cycles. Active cooling (liquid and air cooling) and passive cooling (PCM cooling) are the main strategies to regulate battery temperatures. These techniques regulate the temperature of batteries [17]. Active cooling involves the use of external mechanisms such as fans, pumps, or liquid circulation to remove excess heat, while passive cooling relies on natural heat dissipation without any mechanical intervention.

Air cooling type of active cooling technique, is generally simpler and more cost-effective to implement, compared to PCM cooling systems [18]. Air cooling provides a relatively fast response to changes in temperature. As air is circulated, it can quickly dissipate heat from the battery cells, helping to prevent overheating during sudden temperature spikes or heavy usage. Further, they are suitable for continuous operation without the need for recharging or replacing materials. Air cooling systems can handle a wide range of ambient temperature conditions without significant changes to their performance [19].

Many studies have reported two major weaknesses of the PCM cooling system: low thermal conductivity of the PCM and the low dissipation of the absorbed heat outward (that is, outside the battery). This raised the battery temperature after the PCM completely melted and released its stored latent heat [20].

BTM plays a pivotal role in ensuring battery safety and extending its operational lifespan. To enhance the predictive accuracy of battery pack lifetime estimation, the examination of thermal management systems ought to include capacity fade analysis. Numerous investigations have been attempted to understand the influence of thermal effects on battery capacity. Ramadass et al. [21] conducted experimental assessments on 18650 cylindrical Li-ion batteries, observing a decline in cell voltage correlated with reduced capacity over their operational cycles. This capacity reduction consequently led to a decrease in the battery's energy output. As a result, it is essential to consider not only the maximum temperature threshold but also the impact of capacity fade. Notably, the majority of these studies were conducted under natural convective cooling conditions, without the application of BTM systems. Furthermore, prior research on battery capacity fade did not account for identifying an optimal temperature threshold that could simultaneously enhance safety and extend the battery's lifespan.

The present work focuses on the simulation of a 6-series/2-parallel configuration of 21700 cylindrical Li-ion battery cells with varied electrode chemistries: LCO, NMC, LFP and LMO. The investigation emphasizes on determining an optimal temperature threshold to improve both the longevity and safety of the battery pack, in contrast to the conventional temperature limit of 50deg C commonly used in previous studies.

A numerical model based on the P2D approach is employed to simulate the internal heat transfer within the battery. This model takes into account the generation of ECH during the battery's operation.

To design an effective BTM system, an air cooling method under the category of active cooling techniques, is simulated. The goal is to optimize the BTM system for efficient heat dissipation and temperature control within the battery pack.

The advantages and disadvantages of the proposed method and existing method are given in Table 1.

II. BATTERY MODELING AND CONFIGURATION

To simulate the behaviour of an 21700 cylindrical battery, a 3-D model that couples electrochemical and thermal aspects was created using COMSOL Multiphysics 6.0 software. The model employed Newman's P2D model to predict the generation of heat within the battery [22].

During the discharge process, Li plays a crucial role by facilitating electrochemical redox reaction and diffusing through the surface of negative electrode particles. This action results in the release of electrons and the migration of Li-ions into the electrolyte. Subsequently, Li-ions undergo diffusion into the electrolyte phase as they traverse from the negative electrode to the positive electrode, where a similar process transforms Li into its solid positive phase. Until the battery undergoes recharging, Li remains within the positive electrode particles.

Furthermore, heat is generated by the electrochemical reactions occurring within the internal components of the battery,

TABLE 1. Advantages and disadvantages of the proposed method and existing method.

Proposed Method (Advantages)	Existing Method (Disadvantages)	References
Optimization of Temperature Threshold	Limited Temperature Threshold Exploration	[4], [5]
Incorporation of Varied Electrode Chemistries	Homogeneous Electrode Chemistry Assumption	[2]
Application of Numerical P2D Model	Simplistic Thermal Management Models	[14], [15]
Integration of Safety and Longevity Considerations	Limited Consideration of Safety and Longevity Trade-offs	[27]

leading to an increase in the cell's temperature during its cycling.

Table 2 provides an overview of the essential battery parameters [22] and Table 3 outlines the specific parameters employed in the P2D modeling [22].

In this study, air cooling technique, a type of active thermal management strategy is used to control and maintain the temperature of a battery pack within an optimal range.

Twelve lithium batteries of four electrode chemistries (LCO, NMC, LFP and LMO) as cathode; Graphite, Lithium hexafluoro phosphate ($LiPF_6$), Aluminium (Al) and Copper (Cu) materials as the anode, separator, positive and negative electrode current collector, each with a capacity of 10Ah are used which is connected in a 6-series/2-parallel (6s2p) configuration.

Electrode Chemistries:

LCO -Lithium Cobalt Oxide ($LiCoO_2$)

NMC -Lithium Nickel Manganese Cobalt Oxide ($Li\,Ni_{0.5}Mn_{0.3}Co_{0.2}O_2$)

LFP -Lithium iron phosphate ($LiFePO_4$)

LMO -Lithium Manganese oxide ($LiMn_2O_4$)

Fig. 1 and 2 illustrates the complete setup of geometrical model of the battery module and 6s2p battery pack system with air cooling medium, aluminium connecting wires and active battery material (2 electrode chemistries). The battery pack module is wrapped completely in plastic.

The geometrical parameters of the battery pack modelling are detailed in Table 4.

A. GOVERNING EQUATIONS AND BOUNDARY CONDITIONS

The transport processes of Li-ion within porous particles are governed by the principles of mass conservation and charge conservation. Charge conservation is responsible for determining the phase potentials, $\varphi+$ and φ-, while mass conservation dictates the phase concentrations, denoted as C_e for the electrolyte phase and C_s for the solid (electrode) phase [16], [22]. The conservation equations for both the electrolyte and solid phases can be succinctly summarized as follows [16], [22]:

Solid phase-lithium conservation:

$$\frac{\partial c_s}{\partial t} = \frac{D_s}{r^2}\frac{\partial}{\partial r}\left(r^2\frac{\partial c_s}{\partial r}\right) \tag{1}$$

TABLE 2. Basic parameters of li-ion battery: LCO, NMC, LFP, LMO [22].

Parameters	Value			
	LCO	NMC	LFP	LMO
Nominal Voltage	3.60V	3.70V	3.2V	3.0V
Typical operating range of voltage	3.0-4.2V/cell	3.0-4.2V/cell	3.6-3.65V/cell	3.0-4.2V/cell
Specific Energy	150–200Wh/kg	150–220Wh/kg	90-160Wh/kg	100-150Wh/kg
Charge (C-rate)	0.7–1C; charges to 4.20V	0.7–1C, charges to 4.20V	0.7–1C, charges to 3.7V	0.5-1C charges to 4.30V
Discharge (C-rate)	1C; 2.50V cut off, Discharge above 1C shortens battery life.	1C; 2C possible on some cells; 2.50V cut-off	1C; 2C possible on some cells; 2.8V cut-off	1C; 3V cut-off voltage

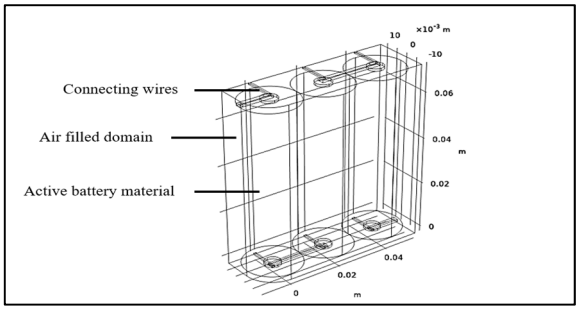

FIGURE 1. Geometry modelling of the battery module [23].

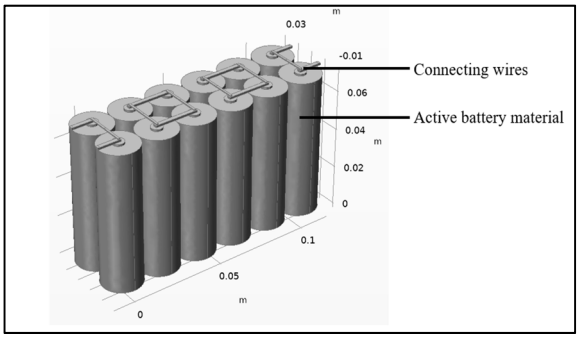

FIGURE 2. Complete setup of the 6s2p battery pack configuration [23].

TABLE 3. Parameters used in the P2D model [22].

Specifications	Positive electrode		Negative electrode (Graphite)	Separator ($LiPF_6$)
Length (m)	55×10^{-6}		55×10^{-6}	30×10^{-6}
Density (kg/m^3)	LCO	2328.5	1347.3	1009
	NMC	4750		
	LFP	1360		
	LMO	4140		
Specific capacity (J/kg.K)	LCO	1269.1	1437.4	1978.2
	NMC	1040		
	LFP	1130		
	LMO	817.5		
Length of Current Collector (m)	Al-130×10^{-6}		Cu-90×10^{-6}	-
Density of Current Collector (kg/m^3)	Al-2770		Cu-8933	-
Specific Capacity of Current Collector (J/kg.K)	Al-875		Cu-385	-
Particle diameter (m)	2.0×10^{-6}		2.5×10^{-6}	-
Maximum solid Li concentration (mol/m^3)	22800		26390	-
Initial electrolyte Li concentration ($molm^3$)	2000		2000	2000
Volume fraction of electrolyte	0.4444		0.357	-
Filler fraction	0.259		0.372	-
Reference diffusivity (m^2/s)	8.0×10^{-14}		3.9×10^{-14}	-
Bruggeman tortuosity exponent	1.5		1.5	1.5
Conductivity (S/m)	0.04		100	-
Reference rate constant	2.0728×10^{-11}		2.0728×10^{-11}	-
Anode charge transfer coefficient	0.5		0.5	
Cathode charge transfer coefficient	0.5		0.5	
Electrolyte diffusivity (m^2/s)	3.0×10^{-11}			
t plus factor	0.22			

Boundary Conditions:

$$\left.\frac{\partial c_s}{\partial r}\right|_{r=0} = 0, -D_s \left.\frac{\partial c_s}{\partial r}\right|_{r=R_S} = \frac{j^{Li}}{a_S F}$$

TABLE 4. Geometry model parameters [23].

Description	Value [mm]
Battery diameter	21
Battery radius	10.5
Battery height	70
Terminal thickness	1
Terminal radius	3
Serial connector depth	2
Serial connector height	1

Electrolyte phase-lithium conservation:

$$\frac{\partial(c_e\varepsilon_e)}{\partial t} = \frac{\partial}{\partial x}\left(D_e^{eff}\frac{\partial c_e}{\partial x}\right) + \frac{1-t_+^0}{F}j^{Li} \tag{2}$$

Boundary Conditions:

$$\left.\frac{\partial c_e}{\partial x}\right|_{x=0} = \left.\frac{\partial c_e}{\partial x}\right|_{x=L_{an}+L_{sep}+L_{ca}} = 0$$

Solid phase-charge conservation:

$$\frac{\partial}{\partial x}\left(\sigma^{eff}\frac{\partial \emptyset_S}{\partial x}\right) = j^{Li} \tag{3}$$

Boundary Conditions:

$$-\sigma^{eff}\left.\frac{\partial \emptyset_S}{\partial x}\right|_{x=0} = -\sigma^{eff}\left.\frac{\partial \emptyset_S}{\partial x}\right|_{x=L_{an}+L_{sep}+L_{ca}} = \frac{I}{A},$$
$$\left.\frac{\partial \emptyset_S}{\partial x}\right|_{x=L_{an}} = \left.\frac{\partial \emptyset_S}{\partial x}\right|_{x=L_{an}+L_{sep}}$$

Electrolyte phase-charge conservation:

$$\frac{\partial}{\partial x}\left(k^{eff}\frac{\partial \emptyset_e}{\partial x}\right) + \frac{\partial}{\partial x}\left(k_D^{eff}\frac{\partial ln(c_e)}{\partial x}\right) + j^{Li} = 0 \tag{4}$$

Boundary Conditions:

$$\left.\frac{\partial \emptyset_e}{\partial x}\right|_{x=0} = \left.\frac{\partial \emptyset_e}{\partial x}\right|_{x=L_{an}+L_{sep}+L_{ca}} = 0$$

The lithium conservation diffusion equation needs to be calculated at every discretized spatial location in the active zone. Butler-Volmer equation is used to pair the charge and species governing equations by defining j^{Li} as a function of over-potential, η as follows [16], [22]:

$$j^{Li} = a_s i_0\left[exp\left(\frac{\alpha_{an}F}{RT}\eta\right) - exp\left(\frac{\alpha_{ca}F}{RT}\eta\right)\right] \tag{5}$$

where η is defined by Eq. (6):

$$\eta = \Phi_s - \Phi_e - U \tag{6}$$

Exchange current density i_0 is given in Eq. (7):

$$i_0 = K_m(C_e)^{\alpha_a}(C_{s,max} - C_{s,e})^{\alpha_a}(C_{s,e})^{\alpha_c} \tag{7}$$

From Eq. (1) to (7), the ionic diffusivity of electrolyte, conductivity, diffusional conductivity, and electrical conductivity in solid phase are defined by Eq. (8) to (14):

$$D_e^{eff} = D_e\varepsilon_e^{\beta} \tag{8}$$

$$K^{eff} = k\varepsilon_e^{\beta} \tag{9}$$

$$\varepsilon_e^{\beta} = \frac{2RTK^{eff}}{F}\left(t_+^0 - 1\right)\left(1 + \frac{dlnf_-^+}{dlnC_e}\right) \tag{10}$$

$$\sigma^{eff} = \sigma\varepsilon_e^{\beta} \tag{11}$$

$$a_s = 3\varepsilon_s/\mathrm{r}_s \tag{12}$$

$$a_s = a_{s,ref}\, exp[-E_d/R(\frac{1}{T} - 1)/T_{ref}] \tag{13}$$

$$k_m = k_{m,ref}\, exp[-E_r/R(\frac{1}{T} - 1)/T_{ref}] \tag{14}$$

B. ENERGY EQUATIONS

The equation for energy balance is as follows:

$$\partial T/\partial t = \alpha(\partial^2 T/\partial x^2 + \partial^2 T/\partial y^2 + \partial^2 T/\partial z^2) + \dot{q}/k \tag{15}$$

where the heat generation term is obtained by:

$$\dot{q} = (\sigma_+ \nabla^2 \varphi_-) + (\sigma_- \nabla^2 \varphi_-) + \dot{q}_{\mathrm{ECH}} \tag{16}$$

$$\dot{q}_{\mathrm{ECH}} = i_p\,(\varphi_+ - \varphi_-) + \int J\left(\frac{T_{ref}\frac{\partial u}{\partial T} - U_{ref}}{L}\right)dx \tag{17}$$

C. STATE ESTIMATIONS, CAPACITY FADE, NUMBER OF CYCLES AND LIFE SPAN OF THE BATTERY-CALCULATION

The state estimations (SOC, DOD and SOH), capacity fade analysis and the total number of cycles and life span [22] of the battery are evaluated based on the following equations given in (18) to (24):

C-rate

The C-rate, defined as the ratio of charging or discharging current to battery capacity, quantifies the rate of energy transfer in batteries, crucial for evaluating charge or discharge speed.

$$\text{C-rate} = \frac{Charging\ Current\ or\ Discharging\ Current}{Q_{battery}} \tag{18}$$

State-of-Charge (SOC)

$$SOC_{initial} + \left(\frac{\int_0^t I\,(t)\,dt}{Q_{battery}}\right) * 100\% \tag{19}$$

Depth of Discharge (DOD)

$$[InitialSOC\ (\%) - FinalSOC\ (\%)] * 100 \tag{20}$$

$$\text{Final SOC} = 100 - \frac{DischargeCurrent}{Q_{battery}} * 100\% \tag{21}$$

Used Capacity

$$Q_{battery}\,(Final) = [InitialSOC\ (\%) - FinalSOC\ (\%)] * Q_{battery} \tag{22}$$

State-of-Health (SOH)

$$\frac{Q_{battery}\,(Final)}{Q_{battery}} * 100\% \tag{23}$$

Capacity Fade

$$\frac{Q_{battery} - Q_{battery}\,(Final)}{Q_{battery}} * 100\% \tag{24}$$

Number of cycles and Life span of the battery

The total number of cycles and life span of the battery (in years) are calculated based on the above equations (18) to (24).

Number of cycles and life span of the battery are evaluated by utilizing the Battery Cycle Life Calculator Application (app) [24], [25].

The following inputs are given to the app are: Cycles per day, Max. SOC, Min. SOC, Charging current, Discharging current, Operating temperature, Battery Capacity and SOH.

Based on the inputs, the total number of cycles of the battery and battery's life span are evaluated.

III. RESULTS AND DISCUSSION

Numerical simulations were conducted using four cathode chemistries (LCO, NMC, LFP and LMO) in an air-cooled battery pack consisting of twelve 21700 Li-ion batteries. The simulations were performed using the COMSOL Multiphysics 6.0 software.

Initially, the mesh analysis is performed for the 6s 2p battery pack model, which enhances the accuracy of the design.

Figure 3 shows the mesh analysis of the designed model.

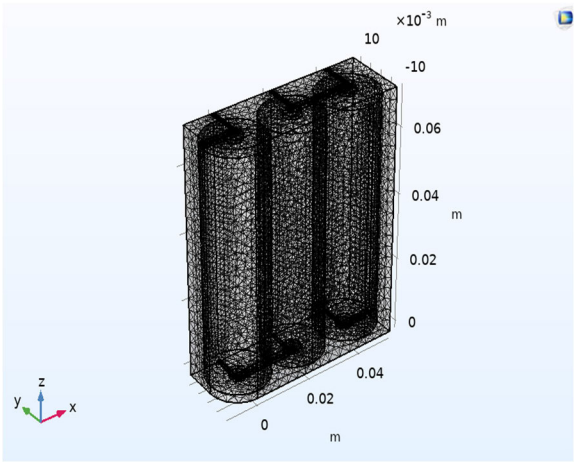

FIGURE 3. Mesh analysis of the 6s 2p battery pack model.

As shown in Figure 3, the battery pack mesh comprises 188 vertex elements, 1534 edge elements, and 77557 elements in total, with 20573 boundary elements. The mesh quality is quantified by the minimum element quality, which is determined to be 0.02601. This meshing process ensures a detailed and accurate representation of the battery pack's geometry, facilitating precise simulations and analyses of its thermal and electrical behavior. The size and free tetrahedral meshing technique employed guarantee optimal discretization, allowing for robust numerical computations and insightful insights into the performance and safety of the battery pack under various operating conditions.

In the study, the following analysis of the battery pack are conducted to evaluate the effectiveness of the battery system with respect to four cathode chemistries (LCO, NMC, LFP and LMO). The analysis are: SOC, Electric potential

(charging and discharging), Heat generation, accumulation and dissipation, Temperature, DOD, Battery Capacity, SOH, Capacity Fade, Number of cycles and life span of the battery.

The analysis is evaluated at: 0.8C rate, 10 Ah-Battery cell capacity, 8A-0.8C current, Temperature-20deg C.

Table 5 shows the nominal, minimum and maximum pack capacity of four electrode chemistries.

TABLE 5. A. Nominal, minimum and maximum pack voltage and capacity-LCO and NMC. B. Nominal, minimum and maximum pack voltage and capacity-LFP and LMO.

(a)

Type	LCO			NMC		
	Nominal	Min	Max	Nominal	Min	Max
Voltage (V)	21.6	18	25.2	22.2	18	25.2
Capacity (Ah)	20	20	20	20	20	20
Total Capacity (Wh)	432	360	504	444	360	504

(b)

Type	LFP			LMO		
	Nominal	Min	Max	Nominal	Min	Max
Voltage (V)	19.2	21.6	21.9	18	18	25.2
Capacity (Ah)	20	20	20	20	20	20
Total Capacity (Wh)	384	432	438	360	360	504

Initially, the SOC of the battery under room temperature (20°C) with respect to different C-rates (0.5C, 0.8C, 1C, 2C, 3C and 4C) [25] for LCO, NMC, LFP and LMO materials are evaluated as shown in Figs. 4a to 4d.

From the analysis, the lithium-ion battery pack using NMC chemistry operates at maximum SOC of 100% under 0.8C, 1C, 2C, 3C and 4C, respectively.

Figs. 5a to 5d and Fig. 6 shows the charging and discharging voltages with respect to SOC and SOD of the battery for LCO, NMC, LFP and LMO chemistries.

Here C and D indicates the charging and discharging voltages of the battery.

The voltage of the lithium battery, starts at a low level and gradually increases as the battery takes in the charge, where the SOC increases steadily during the CC phase.

During the CV phase, battery's SOC approaches 80-90%, where the charger holds the voltage at a fixed level of 4V to 4.2V per cell. Further the battery reaches maximum SOC of 95% to 100% where the charger typically stops the charging process and the voltage is maintained at its maximum limit and the current approaches zero.

Similarly, in the discharging voltage phase of the lithium battery, starts with the CC phase, and the voltage starts at 4V to 4.2V and gradually decreases as the battery discharges. There is a steady decrease in SOC during this phase. As the battery's SOC approaches 20%, the voltage starts to drop rapidly. In the CV phase, the voltage is stable, but the current decreases as the battery discharges further.

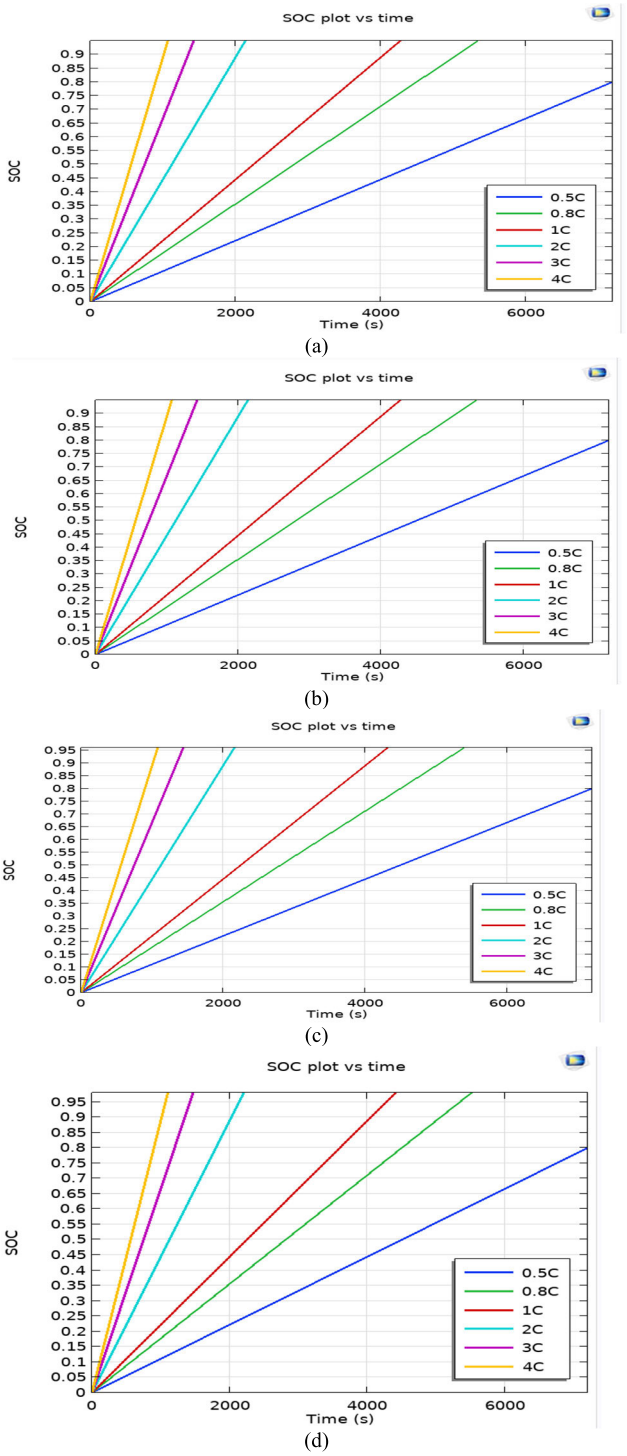

FIGURE 4. SOC (a) LCO, (b) NMC, (c) LFP, (d) LMO.

From the analysis, the NMC battery chemistry at 0.8C rate performs better with maximum charging voltage of 4.2V and discharges safely around 2.2V, more effective in comparison to other chemistries respectively.

Figs. 7 to 8 shows the heat generation and accumulation [26] of the battery pack at different C-rates (0.5C, 0.8C, 1C, 2C, 3C and 4C). The maximum heat generation and

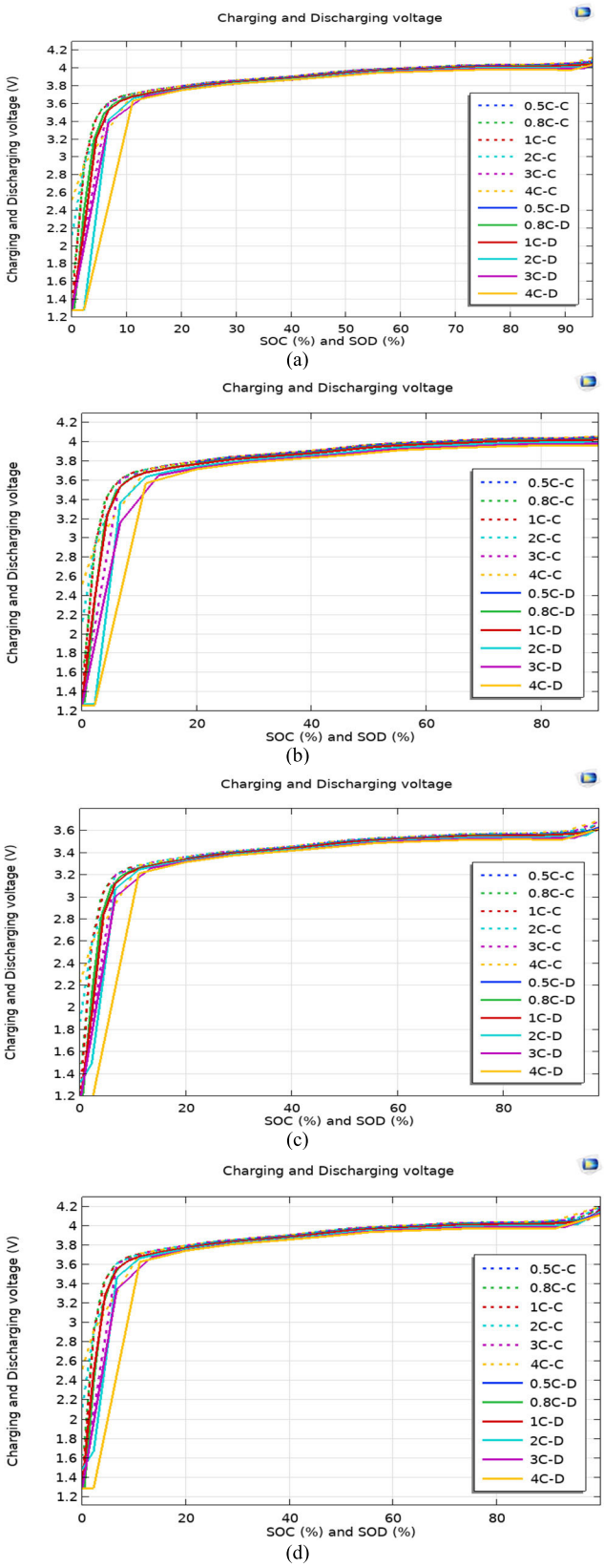

FIGURE 5. Charging and discharging voltage (a) LCO, (b) NMC, (c) LFP, (d) LMO.

minimum heat accumulation has been attained at 4C rate and 0.5C rate by the four cathode chemistries.

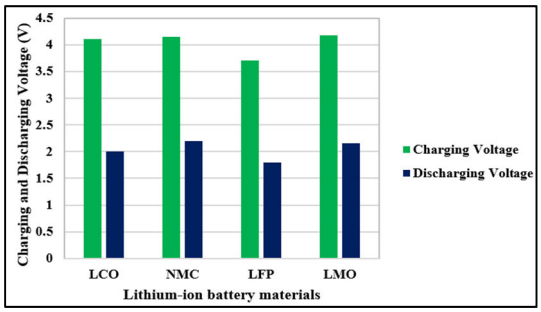

FIGURE 6. Charging and discharging voltage-0.8C rate.

From the analysis, the NMC electrode chemistry have effectively dissipated the maximum amount of heat from the battery pack with minimum heat accumulation. The NMC electrode chemistry has generated maximum heat of 102.5W with the corresponding minimum heat accumulation of 0.0128W at 4C rate, which is more effective in comparison to other chemistries.

Moreover, the heat generation decreases with reduced C-rate. The minimum heat generation is obtained at C-rates, 0.5C and 0.8C of about 0.5W and 6.8W by the NMC electrode chemistry. The corresponding heat accumulation are, 0.0005W and 0.0016W respectively.

Further, the maximum heat has been accumulated by the LCO cathode chemistry of 10.2W, which is more in comparison to NMC, LFP and LMO chemistries.

The heat dissipation from the battery pack at different C-rates with respect to four cathode chemistries is shown in Figure 9. The maximum amount of heat has been dissipated using the NMC battery chemistry at C-rates, 0.5C to 4C.

From the evaluations, with respect to C-rates, the NMC cathode chemistry has dissipated maximum amount of heat of 102.48W at 4C rate respectively.

In comparison to LCO, LFP and LMO chemistries, the NMC cathode chemistry has dissipated maximum amount of heat with minimum heat accumulation in the battery pack respectively.

Figs. 10a to 10d shows the temperature analysis of the battery pack with respect to four battery chemistries, in which the NMC battery generates optimal temperature range at 0.8 C rate between 21.3deg C and 32.8deg C respectively.

The LCO, LFP and LMO battery chemistries show poor performance with maximum temperature of about 44.2deg C, 44deg C and 42.1deg C, which is due to the maximum heat accumulation and minimum heat dissipation in the lithium battery pack, respectively.

Fig. 11 shows the temperature distribution of NMC battery in the pack, where the solution data has been mirrored twice to illustrate the temperature of the full 6s2p pack. The innermost parts of the pack experience a temperature about 2deg C higher than the outermost parts. The minimum and maximum temperature of the battery pack is attained by the NMC battery of about 21.3deg C and 32.8deg C.

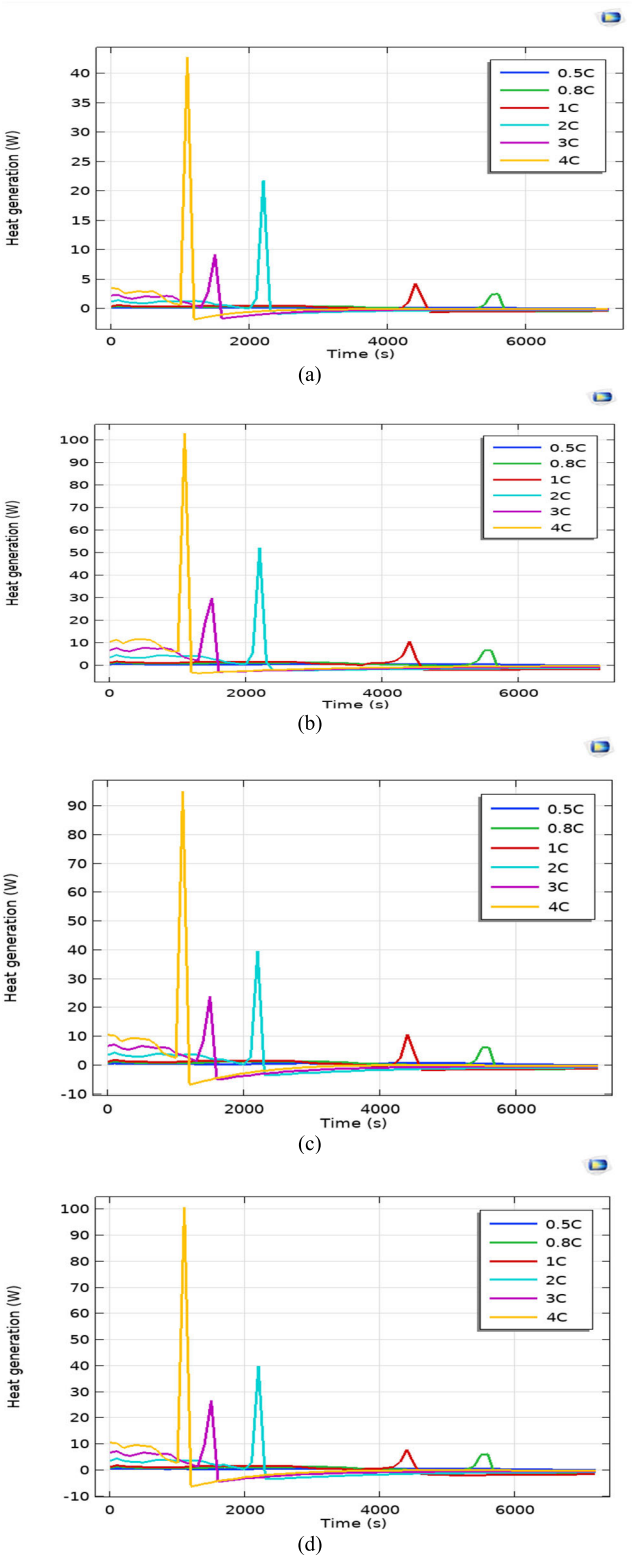

FIGURE 7. Heat generation (a) LCO, (b) NMC, (c) LFP, (d) LMO.

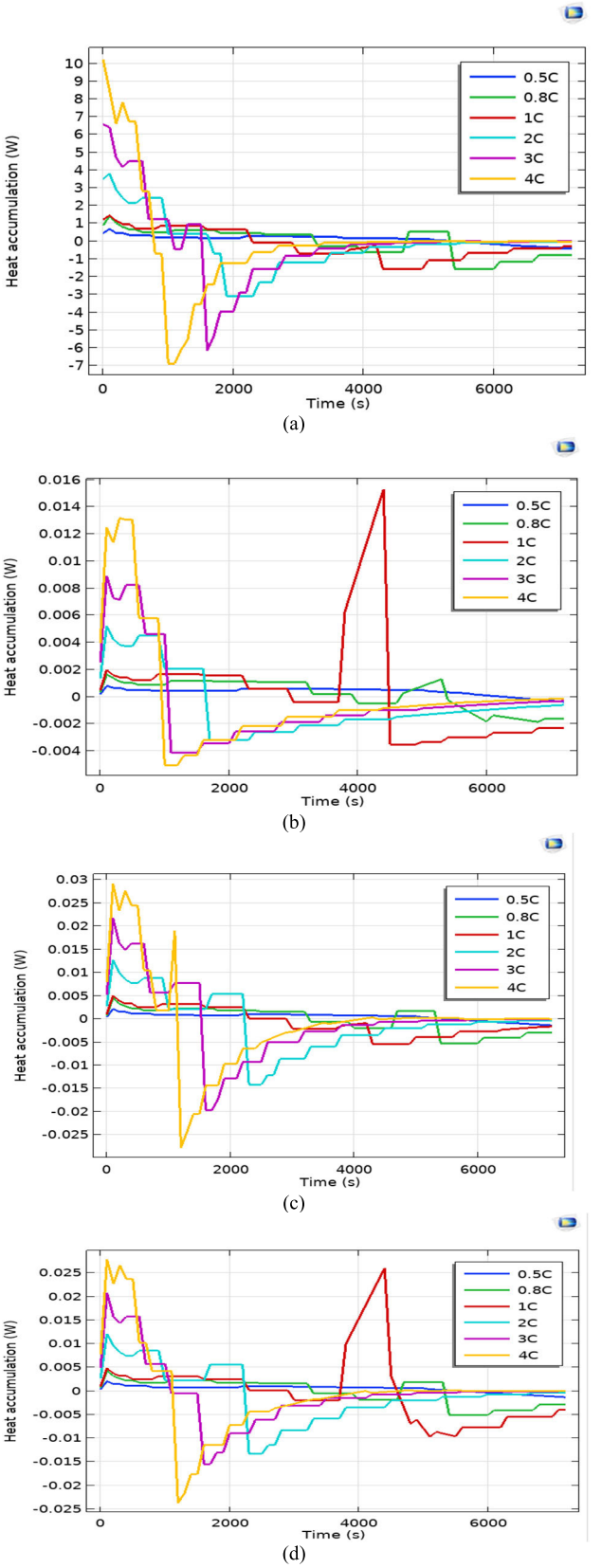

FIGURE 8. Heat accumulation (a) LCO, (b) NMC, (c) LFP, (d) LMO.

Hence, through an analysis encompassing, SOC, voltage, heat generation, accumulation, dissipation and temperature analysis of the battery, the 0.8C rate proves to be the optimal choice. Operating at maximum SOC and maintaining charging and discharging voltages within the specified range, this

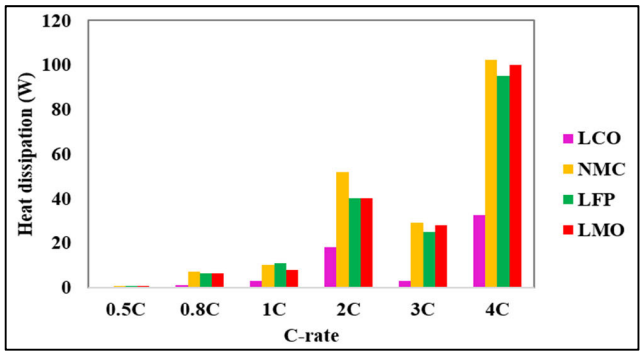

FIGURE 9. Heat dissipation.

approach minimizes heat generation and accumulation while optimizing dissipation. The temperature analysis further confirms that this strategy establishes an ideal temperature limit, ensuring the battery operates at its maximum capacity.

Further analysis is carried out with 0.8 C rate throughout the article.

SOH and DOD of the battery at 0.8C rate are evaluated based on the equations (18) to (24) for battery chemistries, which are shown in Figure 11.

From the analysis, the minimum SOH and DOD has been generated by the LCO chemistry of about 75%. Maximum amount of SOH and DOD of 80% has been produced by the NMC battery. This indicates that the battery's current capacity and efficiency align with its expected performance at the given DOD. Maximum SOH and DOD minimizes wasted energy and capacity, reducing environmental impact and enhancing sustainability.

Fig. 13 shows the battery capacity (used and unused) for LCO, NMC, LFP and LMO chemistries. The minimum amount of capacity has been used by the LCO battery of about 7.5Ah, with 2.5Ah of unused capacity. Maximum capacity of 8Ah has been used by the NMC battery chemistry, with 2Ah of unused capacity.

NMC chemistry has utilized the battery capacity to its fullest extent.

Fig. 14 shows the capacity fade analysis of the battery for LCO, NMC, LFP and LMO chemistries.

NMC battery has attained maximum amount of capacity fade (Capacity loss) of 80%, with current effective capacity of 20%. The minimum capacity fade is attained by LCO battery of 75%.

With respect to the above analysis, the total number of cycles of the battery and the battery life span are calculated using the Battery Cycle Life calculator app [24], [25], which are shown in Figs. 15 and 16.

Based on [24] and [25], the total number of charging and discharging cycles of the battery for LCO and NMC chemistries are 2160 and 1133 cycles, respectively. LFP and LMO have attained 1966 and 1522 cycles, respectively.

The minimum battery life span has been attained by the NMC chemistry of about 3.9 years, whereas the maximum life span has been achieved by the LCO chemistry of about 7.9 years respectively.

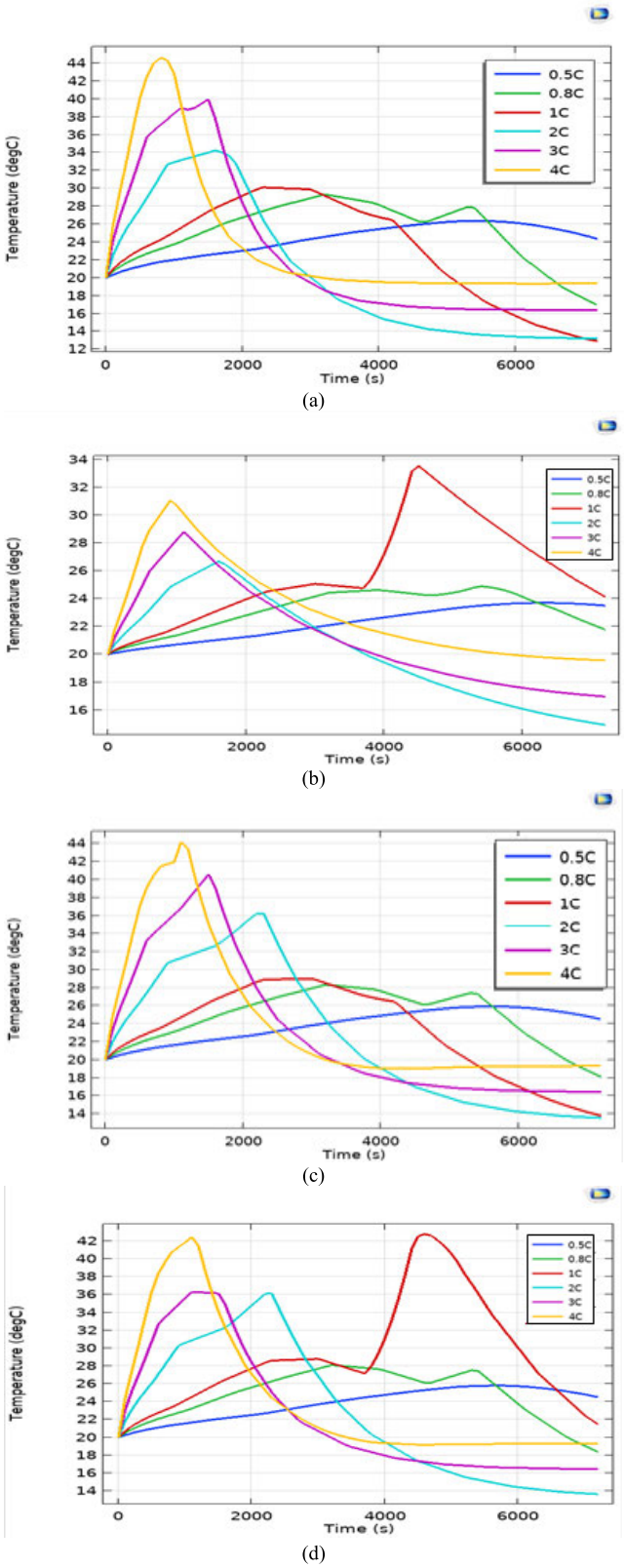

FIGURE 10. Temperature analysis (a) LCO, (b) NMC, (c) LFP, (d) LMO.

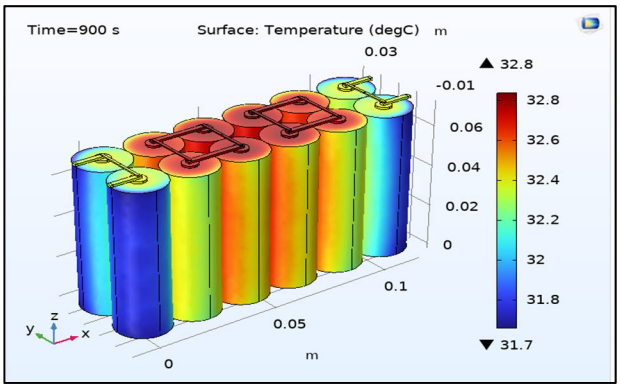

(a)

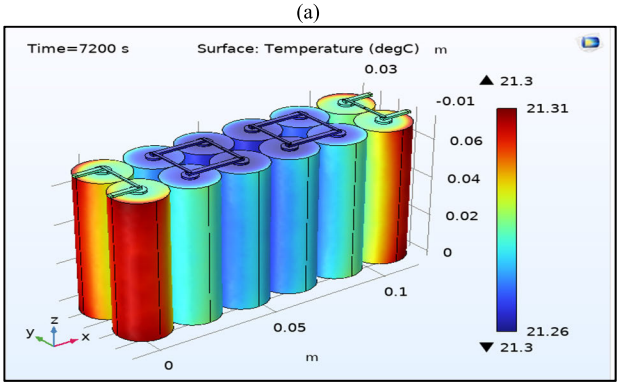

(b)

FIGURE 11. NMC battery (a) 900s, (b) 7200s.

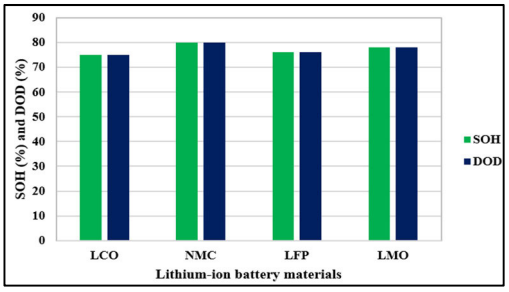

FIGURE 12. SOH(%) and DOD (%).

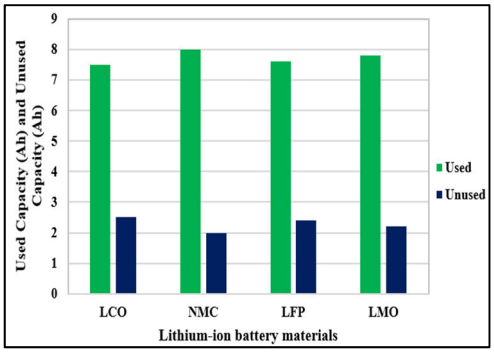

FIGURE 13. Battery capacity (Ah) (Used and Unused capacity).

From the analysis of capacity fade, number of cycles of the battery and battery's life span, the NMC battery chemistry has attained maximum capacity loss with minimum number of cycles and lower life span of battery.

The maximum capacity fade in the lithium battery pack can be due to the cycling stress, a common occurrence in battery use, induce stress on the NMC electrodes. The mechanical stress can lead to structural changes and degradation, contributing to capacity fade. Over time, the active materials in the electrodes may undergo degradation due to chemical reactions and phase changes. This degradation contributes to the loss of capacity [27].

Despite a lower lifespan and cycle count, along with considerable capacity loss [27], the NMC battery attains maximum charging and discharging voltages within permissible

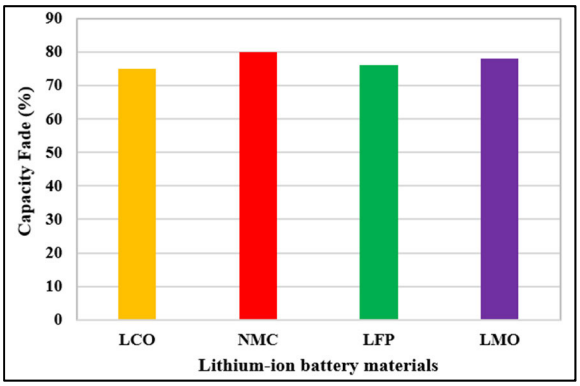

FIGURE 14. Capacity fade analysis battery capacity (Ah) (Used and Unused capacity).

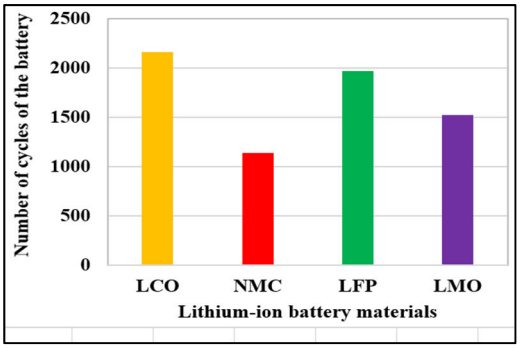

FIGURE 15. Number of cycles of the battery.

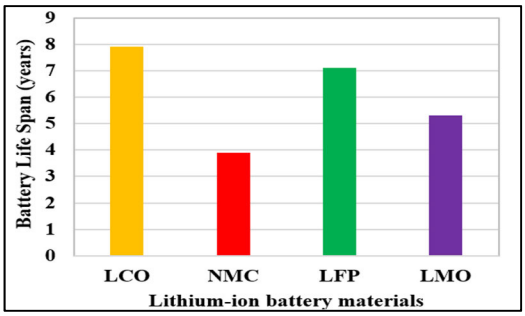

FIGURE 16. Battery life span.

limits. It excels in the 6s2p battery pack analysis, maintaining nominal voltage limits (charging-4.2V, discharging-2.2V) and efficiently utilizing its 8Ah storage capacity. The NMC battery also operates within optimal temperature limits (21.3deg C to 32.8deg C), demonstrating superior heat dissipation compared to LCO, LFP, and LMO chemistries.

A comparison is made between the results of the proposed work and the existing work based upon the following parameters: Charging and Discharging voltage, Temperature and Capacity Fade, which are shown in Table 6. From the above results and analysis, these are the major parameters, which affects the battery's life and performance, hence they are considered for comparison.

From the analysis, the results of the proposed work are effective in comparison to existing literature with maximum charging and discharging voltage, optimal temperature, and minimum capacity fade respectively.

TABLE 6. Comparison analysis - proposed work and existing work.

Parameters	This Work	Existing Work		
		[6]	[3]	[7]
Charging Voltage (V)	4.2	4	3.6	4.2
Discharging Voltage (V)	2.2	1	2.7	3
Temperature (deg C)	32.8	41.5	66	52
Capacity Fade (%)	80	90	85	82

IV. CONCLUSION

The present study develops a BTM technique using air cooling to enhance the efficiency of a cylindrical lithium-ion battery pack (6s 2p configuration). The system employs positive electrodes (LCO, NMC, LFP, and LMO), negative electrode (graphite), and separator ($LiPF_6$). Utilizing a P2D model and three-dimensional computational fluid dynamics, the evaluation includes thermal simulation, optimal temperature thresholds, SOC and SOH estimations, cycle life, and battery lifespan. NMC in a 6s 2p configuration with air cooling attains an optimal temperature range of 21.3deg C to 32.8deg C at 100% SOC and 80% SOH, dissipating a maximum heat of 102.48W. After 1000 cycles, an 80% capacity loss is observed for an 8Ah battery with a lifespan of 3.9 years, indicating minimal impact on charge/discharge cycles.

REFERENCES

[1] U. Iraola, I. Aizpuru, L. Gorrotxategi, J. M. C. Segade, A. E. Larrazabal, and I. Gil, "Influence of voltage balancing on the temperature distribution of a li–ion battery module," *IEEE Trans. Energy Convers.*, vol. 30, no. 2, pp. 507–514, Jun. 2015.

[2] K. Murashko, J. Pyrhönen, and L. Laurila, "Three-dimensional thermal model of a lithium ion battery for hybrid mobile working machines: Determination of the model parameters in a pouch cell," *IEEE Trans. Energy Convers.*, vol. 28, no. 2, pp. 335–343, Jun. 2013.

[3] K. Smith and C.-Y. Wang, "Power and thermal characterization of a lithium-ion battery pack for hybrid-electric vehicles," *J. Power Sources*, vol. 160, no. 1, pp. 662–673, Sep. 2006, doi: 10.1016/j.jpowsour.2006.01.038.

[4] A. Väyrynen and J. Salminen, "Lithium ion battery production," *J. Chem. Thermodyn.*, vol. 46, pp. 80–85, Mar. 2012, doi: 10.1016/j.jct.2011.09.005.

[5] K. Jiang, G. Liao, E. Jiaqiang, F. Zhang, J. Chen, and E. Leng, "Thermal management technology of power lithium-ion batteries based on the phase transition of materials: A review," *J. Energy Storage*, vol. 32, Dec. 2020, Art. no. 101816, doi: 10.1016/j.est.2020.101816.

[6] U. S. Kim, J. Yi, C. B. Shin, T. Han, and S. Park, "Modelling the thermal behaviour of a lithium-ion battery during charge," *J. Power Sources*, vol. 196, no. 11, pp. 5115–5121, Jun. 2011, doi: 10.1016/j.jpowsour.2011.01.103.

[7] N. Baba, H. Yoshida, M. Nagaoka, C. Okuda, and S. Kawauchi, "Numerical simulation of thermal behavior of lithium-ion secondary batteries using the enhanced single particle model," *J. Power Sources*, vol. 252, pp. 214–228, Apr. 2014, doi: 10.1016/j.jpowsour.2013.11.111.

[8] S. Panchal, M. Mathew, R. Fraser, and M. Fowler, "Electrochemical thermal modeling and experimental measurements of 18650 cylindrical lithium-ion battery during discharge cycle for an EV," *Appl. Thermal Eng.*, vol. 135, pp. 123–132, May 2018, doi: 10.1016/j.applthermaleng.2018.02.046.

[9] A. Fotouhi, D. J. Auger, K. Propp, S. Longo, and M. Wild, "A review on electric vehicle battery modelling: From lithium-ion toward lithium–sulphur," *Renew. Sustain. Energy Rev.*, vol. 56, pp. 1008–1021, Apr. 2016, doi: 10.1016/j.rser.2015.12.009.

[10] X. Lin, H. E. Perez, S. Mohan, J. B. Siegel, A. G. Stefanopoulou, Y. Ding, and M. P. Castanier, "A lumped-parameter electro-thermal model for cylindrical batteries," *J. Power Sources*, vol. 257, pp. 1–11, Jul. 2014, doi: 10.1016/j.jpowsour.2014.01.097.

[11] X. Zhang, R. Klein, A. Subbaraman, S. Chumakov, X. Li, J. Christensen, C. Linder, and S. U. Kim, "Evaluation of convective heat transfer coefficient and specific heat capacity of a lithium-ion battery using infrared camera and lumped capacitance method," *J. Power Sources*, vol. 412, pp. 552–558, Feb. 2019, doi: 10.1016/j.jpowsour.2018.11.064.

[12] W. Allafi, C. Zhang, K. Uddin, D. Worwood, T. Q. Dinh, P. A. Ormeno, K. Li, and J. Marco, "A lumped thermal model of lithium-ion battery cells considering radiative heat transfer," *Appl. Thermal Eng.*, vol. 143, pp. 472–481, Oct. 2018, doi: 10.1016/j.applthermaleng.2018.07.105.

[13] M. Chen, F. Bai, W. Song, J. Lv, S. Lin, Z. Feng, Y. Li, and Y. Ding, "A multilayer electro-thermal model of pouch battery during normal discharge and internal short circuit process," *Appl. Thermal Eng.*, vol. 120, pp. 506–516, Jun. 2017, doi: 10.1016/j.applthermaleng.2017.03.135.

[14] J. Xie, Z. Li, J. Jiao, and X. Li, "Lumped-parameter temperature evolution model for cylindrical li–ion batteries considering reversible heat and propagation delay," *Measurement*, vol. 173, Mar. 2021, Art. no. 108567, doi: 10.1016/j.measurement.2020.108567.

[15] M. Doyle, T. F. Fuller, and J. Newman, "Modeling of galvanostatic charge and discharge of the lithium/polymer/insertion cell," *J. Electrochem. Soc.*, vol. 140, no. 6, pp. 1526–1533, Jun. 1993.

[16] L. H. Saw, Y. Ye, and A. A. O. Tay, "Electrochemical–thermal analysis of 18650 lithium iron phosphate cell," *Energy Convers. Manage.*, vol. 75, pp. 162–174, Nov. 2013, doi: 10.1016/j.enconman.2013.05.040.

[17] R. D. Widyantara, M. A. Naufal, P. L. Sambegoro, I. P. Nurprasetio, F. Triawan, D. W. Djamari, A. B. D. Nandiyanto, B. A. Budiman, and M. Aziz, "Low-cost air-cooling system optimization on battery pack of electric vehicle," *Energies*, vol. 14, no. 23, p. 7954, Nov. 2021, doi: 10.3390/en14237954.

[18] C. Yang, H. Xi, and M. Wang, "Structure optimization of air cooling battery thermal management system based on lithium-ion battery," *J. Energy Storage*, vol. 59, Mar. 2023, Art. no. 106538, doi: 10.1016/j.est.2022.106538.

[19] P. Saechan and I. Dhuchakallaya, "Numerical study on the air-cooled thermal management of lithium-ion battery pack for electrical vehicles," *Energy Rep.*, vol. 8, pp. 1264–1270, Apr. 2022, doi: 10.1016/j.egyr.2021.11.089.

[20] J. Kim, J. Oh, and H. Lee, "Review on battery thermal management system for electric vehicles," *Appl. Thermal Eng.*, vol. 149, pp. 192–212, Feb. 2019, doi: 10.1016/j.applthermaleng.2018.12.020.

[21] P. Ramadass, B. Haran, R. White, and B. N. Popov, "Capacity fade of Sony 18650 cells cycled at elevated temperatures," *J. Power Sources*, vol. 112, no. 2, pp. 606–613, Nov. 2002.

[22] P. G. Zadeh, E. Gholamalizadeh, Y. Wang, and J. D. Chung, "Electrochemical modeling of a thermal management system for cylindrical lithium-ion battery pack considering battery capacity fade," *Case Stud. Thermal Eng.*, vol. 32, Apr. 2022, Art. no. 101878, doi: 10.1016/j.csite.2022.101878.
[23] *Thermal Distribution in a Pack of Cylindrical Batteries*, COMSOL Multiphysics Version 6.0, COMSOL AB, Stockholm, Sweden, 2021.
[24] *Battery Cycle Life Calculator*. Accessed: Sep. 2023. [Online]. Available: https://app.calculoid.com/#/calculator/846
[25] M. Valentin, J. de Hoog, B. Marcus, A. Vishwanath, and S. Kalyanaraman, "A multi-factor battery cycle life prediction methodology for optimal battery management," in *Proc. ACM 6th Int. Conf. Future Energy Syst.*, Jul. 2015, pp. 57–66, doi: 10.1145/2768510.2768532.
[26] S. M. R. Islam and S.-Y. Park, "Quantification of heat loss for different charging profiles in a li–ion battery," *IEEE Trans. Energy Convers.*, vol. 36, no. 3, pp. 1831–1840, Sep. 2021.
[27] T. Sun, S. Jiang, X. Li, Y. Cui, X. Lai, X. Wang, Y. Ma, and Y. Zheng, "A novel capacity estimation approach for lithium-ion batteries combining three-parameter capacity fade model with constant current charging curves," *IEEE Trans. Energy Convers.*, vol. 36, no. 3, pp. 2574–2584, Sep. 2021.

P. MANGAIYARKARASI was born in Chennai, Tamil Nadu, India, in May 1994. She received the bachelor's and master's degrees in electrical and electronics engineering from Anna University, Chennai, in 2015 and 2017, respectively, and the Ph.D. degree in electrical and electronics engineering, in 2022. Since 2022, she has been a Postdoctoral Researcher with the Department of Engineering Design, Indian Institute of Technology (IIT) Madras, Chennai. Her research interests include battery management systems, electric vehicles, finite element analysis, microelectronics, energy harvesting and storage, and artificial intelligence.

R. JAYAGANTHAN was born in Thuraiyur, Tiruchirappalli, Tamil Nadu, in June 1968. He received the Ph.D. degree in materials engineering from Indian Institute of Science, Bengaluru, in 1998. Since 2015, he has been a Professor with the Department of Engineering Design, Indian Institute of Technology (IIT) Madras. He was a former Alexander Von Humboldt Fellow and a Visiting Scientist with the Max Planck Institute for Intelligent Systems, Stuttgart, Germany. His current research interests include battery engineering, additive manufacturing, fatigue and fracture mechanics, FEA, data analytics in manufacturing, and mechanical design.